J|A|C|S ARTICLES

Published on Web 12/08/2008

Structural Rearrangements of Membrane Proteins Probed by Water-Edited Solid-State NMR Spectroscopy

Christian Ader,[†] Robert Schneider,[‡] Karsten Seidel,[‡] Manuel Etzkorn,[‡] Stefan Becker,[‡] and Marc Baldus*,[†]

Bijvoet Center for Biomolecular Research, Utrecht University, Padualaan 8, 3584 CH Utrecht, The Netherlands, and Department of NMR-based Structural Biology, Max Planck Institute for Biophysical Chemistry, Am Fassberg 11, 37077 Göttingen, Germany

Received August 9, 2008; E-mail: m.baldus@uu.nl

Abstract: We show that water-edited solid-state NMR spectroscopy allows for probing global protein conformation and residue-specific solvent accessibility in a lipid bilayer environment. The transfer dynamics can be well described by a general time constant, irrespective of protein topology and lipid environment. This approach was used to follow structural changes in response to protein function in the chimeric potassium channel KcsA-Kv1.3. Data obtained as a function of pH link earlier biochemical data to changes in protein structure in a functional bilayer setting.

Introduction

Membrane proteins control fundamental biological processes including protein synthesis and signal transduction. Their function is often intimately related to structural changes triggered by external stimuli and modulated by the surrounding membrane, making membrane proteins an important target for pharmacological research. Diffraction methods provide increasing insight into membrane protein structure but require the use of protein crystals (see, e.g., refs 1 and 2). While biophysical methods such as FRET and EPR offer structural insight at the nanometer scale,[3,4] solid-state NMR (ssNMR) can be used to study very accurately local structural rearrangements in a membrane environment. Advanced techniques such as ^{19}F or nitroxide spin labeling can extend the NMR-detectable distance range beyond the 3−8 Å range limit if their effect on protein structure is minimized.[5−7]

ssNMR pulse schemes adapting the Goldman−Shen[8] experiment were, in a complementary manner, used to globally probe membrane protein topology in peptides and proteins reconstituted in a native lipid environment.[9−12] In these experiments, the resulting one- or two-dimensional ssNMR data sets show signals arising from polarization transfer between water and proteins. In the case of a microcrystalline protein, chemical exchange was identified as a major pathway for magnetization transfer from water to the surface of a solid protein, and it was also confirmed that polarization transfer by NOE takes place. While the presence of intermolecular dipolar polarization transfer could not be directly demonstrated in this study, it can also not be strictly excluded (Figure 1).[13,14] A principal question, therefore, has remained to which extent the data interpretation of these water-edited experiments, in particular the rate of magnetization transfer between water and the protein, depends on the details of the system of interest.

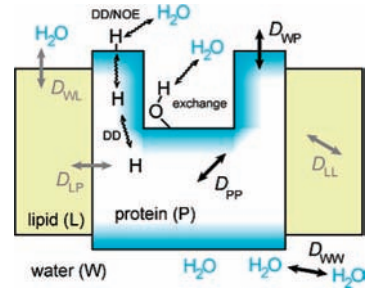

Figure 1. Schematic representation of diffusion pathways and possible mechanisms for magnetization transfer between and among water and protein protons (DD, direct dipolar interaction; NOE, nuclear Overhauser effect; exchange, chemical exchange processes involving fast exchanging protein protons). Relevant diffusion coefficients describing magnetization transfer between and among the different phases are indicated as D_{ij}, where i and j can be W (water), P (protein), and L (lipid).

[†] Utrecht University.
[‡] Max Planck Institute for Biophysical Chemistry.

(1) MacKinnon, R. *Angew. Chem., Int. Ed.* **2004**, *43*, 4265–4277.
(2) Shimizu, H.; Iwamoto, M.; Konno, T.; Nihei, A.; Sasaki, Y. C.; Oiki, S. *Cell* **2008**, *132*, 67–78.
(3) Jares-Erijman, E. A.; Jovin, T. M. *Nat. Biotechnol.* **2003**, *21*, 1387–1395.
(4) Klare, J. P.; Gordeliy, V. I.; Labahn, J.; Buldt, G.; Steinhoff, H.-J.; Engelhard, M. *FEBS Lett.* **2004**, *564*, 219–224.
(5) Ulrich, A. S. *Prog. Nucl. Magn. Reson. Spectrosc.* **2005**, *46*, 1–21.
(6) Liang, B.; Bushweller, J. H.; Tamm, L. K. *J. Am. Chem. Soc.* **2006**, *128*, 4389–4397.
(7) Hong, M. *J. Phys. Chem. B* **2007**, *111*, 10340–10351.
(8) Goldman, M.; Shen, L. *Phys. Rev.* **1966**, *144*, 321–331.
(9) Kumashiro, K. K.; Schmidt-Rohr, K.; Murphy, O. J.; Ouellette, K. L.; Cramer, W. A.; Thompson, L. K. *J. Am. Chem. Soc.* **1998**, *120*, 5043–5051.
(10) Gallagher, G. J.; Hong, M.; Thompson, L. K. *Biochemistry* **2004**, *43*, 7899–7906.
(11) Huster, D.; Yao, X.; Hong, M. *J. Am. Chem. Soc.* **2002**, *124*, 874–883.
(12) Etzkorn, M.; Martell, S.; Andronesi, O. C.; Seidel, K.; Engelhard, M.; Baldus, M. *Angew. Chem., Int. Ed.* **2007**, *46*, 459–462.
(13) Lesage, A.; Emsley, L.; Penin, F.; Bockmann, A. *J. Am. Chem. Soc.* **2006**, *128*, 8246–8255.
(14) Lesage, A.; Gardiennet, C.; Loquet, A.; Verel, R.; Pintacuda, G.; Emsley, L.; Meier, B. H.; Böckmann, A. *Angew. Chem., Int. Ed.* **2008**, *47*, 5851–5854.

10.1021/ja806306e CCC: $40.75

Using membrane proteins of different topology and in different membrane environments, we show in the following that one-dimensional water-edited ssNMR experiments can be well described by a general, effective diffusion coefficient for magnetization transfer from water to protein. Combining experimental results with three-dimensional lattice calculations supports the notion that different membrane protein systems are directly comparable in terms of the ratio between solvent-exposed surface and protein volume. Using the potassium channel KcsA-Kv1.3 as an example, we show that these dependencies provide a useful framework to study the protein−water interface on a residue-specific level. In addition, we demonstrate how these experiments can be used as a straightforward means to follow structural rearrangements related to channel gating in a functional membrane environment.

Materials and Methods

Sample Preparation. Sensory rhodopsin II from *Natronomonas pharaonis* (NpSRII), a monomeric phospholamban mutant (AFA-PLN), and the chimeric potassium channel KcsA-Kv1.3 were prepared as described previously.[12,15,16] pH titration for KcsA-Kv1.3 was performed by washing the samples three times with 100 mM citric acid/citrate buffer or 50 mM phosphate buffer adjusted to the desired pH.

Solid-State NMR Experiments and Analysis. All 1D and build-up experiments (Figure 2a, b) were recorded on a 400 MHz instrument (Bruker Biospin). A 3 ms Gaussian pulse and a T_2 filter containing two delays (τ) of 1 ms were used for selective water excitation. The cross-polarization contact time was set to 700 μs. The field strength for SPINAL64[17] proton decoupling was typically between 70 and 83 kHz. All ssNMR experiments were performed at 280 K using a 4 mm triple-resonance MAS (magic angle spinning) probe and an MAS rate of 6.5 kHz. 2D water-edited (^{13}C, ^{13}C) correlation experiments (Figure 2c) were performed at 600 MHz proton frequency using an MAS rate of 9.375 kHz and a temperature of 280 K. Spin-diffusion times t_m and τ_m were set to 2.5 and 20 ms, respectively. Other experimental parameters were similar as described above. To analyze the ^{13}C detected water-edited build-up experiments, peak integrals for the spectral region from 80 ppm to 0 ppm were obtained and corrected for water T_1 relaxation by multiplication with $\exp(t_m/T_1)$. ^{1}H spin−lattice relaxation times of the water and the tail CH_2 lipid signals were measured using standard NMR inversion recovery sequences.

Theoretical Background. Starting from the diffusion equation for z magnetization $M(\vec{r},t_m)$

$$\frac{\partial M(\vec{r},t_m)}{\partial t_m} = \vec{\nabla}\cdot\{D(\vec{r})\vec{\nabla}M(\vec{r},t_m)\} \quad (1)$$

magnetization transfer from water to protein can be described assuming a semi-infinite two-phase system with a uniform ^{1}H spin density.[18] At time zero, the magnetization is homogeneously distributed in phase A (water in our case) and zero in phase B (protein in our case). Diffusion of magnetization from phase A to B for a system with homogeneous diffusibility can then be described as follows

$$\frac{I_B(t_m)}{I_B(t_m\rightarrow\infty)} = \sqrt{\frac{Dt_m}{\pi}}\frac{1}{f_A f_B}\frac{S_{AB}^{tot}}{V^{tot}} - O\left(\sqrt{t_m^2}\right) \quad (2)$$

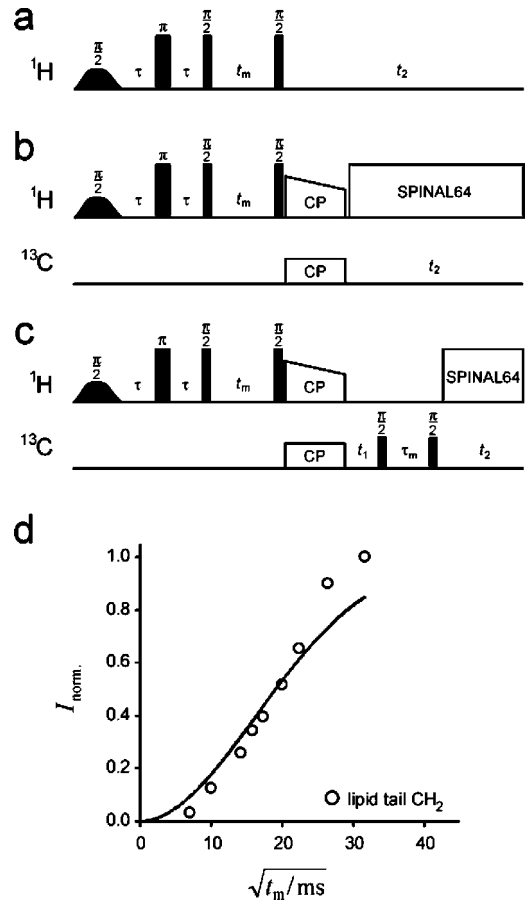

Figure 2. (a) Pulse scheme for a ^{1}H-detected 1D water-edited cross-polarization experiment. (b) Pulse scheme for a ^{13}C-detected 1D water-edited cross-polarization experiment. After an initial Gaussian 90° pulse on resonance with the ^{1}H water signal, a ^{1}H T_2 filter (τ) leads to the selection of mobile water ^{1}H magnetization. A subsequent longitudinal spin diffusion unit (t_m) establishes polarization transfer to protein protons. Transferred magnetization is read out after a cross-polarization step on ^{13}C nuclei. (c) Pulse scheme for 2D water-edited dipolar (^{13}C, ^{13}C) correlation spectroscopy including an additional (^{13}C, ^{13}C) spin-diffusion unit of duration τ_m. (d) Normalized intensities for the ^{1}H lipid tail CH_2 resonance at 0.9 ppm of asolectin liposomes, obtained for ^{1}H detected 1D water-edited experiments, plotted against the square root of mixing time. The solid line represents the simulated build-up curve based on lattice calculations using a water to lipid diffusion coefficient for magnetization transfer of 0.001 nm^2/ms and a lipid to lipid diffusion coefficient of 0.016 nm^2/ms.

In eq 2, $I_B(t_m\rightarrow\infty)$ represents B (protein) magnetization under equilibrium conditions. Furthermore, D is the diffusion coefficient and f_A, f_B stand for the volume fractions of phases A and B, respectively. In addition, S_{AB}^{tot} is the total interface area between A and B, and V^{tot} represents the total sample volume. $O(\sqrt{t_m}^2)$is a term quadratic in $\sqrt{t_m}$ and will be ignored in the following. Assuming that phase A (water) takes a major fraction of the sample volume and the total volume of phase B (protein) is small in contrast, eq 2 reduces to

$$\frac{I_B(t_m)}{I_B(t_m\rightarrow\infty)} \approx \sqrt{\frac{Dt_m}{\pi}}\frac{S_{AB}^{tot}}{V_B} \quad (3)$$

because $f_A \approx 1$.

Notably, proteoliposome samples discussed below do not fulfill the assumption of homogeneous diffusibility as postulated for the derivation of eq 3. Thus, the diffusion coefficient D in eq 3 represents an effective diffusion parameter D_{eff} comprising all diffusion coefficients relevant for the observed magnetization transfer in the system.

(15) Andronesi, O. C.; Becker, S.; Seidel, K.; Heise, H.; Young, H. S.; Baldus, M. *J. Am. Chem. Soc.* **2005**, *127*, 12965–12974.
(16) Lange, A.; Giller, K.; Hornig, S.; Martin-Eauclaire, M.-F.; Pongs, O.; Becker, S.; Baldus, M. *Nature* **2006**, *440*, 959–962.
(17) Fung, B. M.; Khitrin, A. K.; Ermolaev, K. *J. Magn. Reson.* **2000**, *142*, 97–101.
(18) Schmidt-Rohr, K.; Spiess, H. W. *Multidimensional Solid-State NMR and Polymers*, 1st ed.; Academic Press: London/San Diego, 1994.

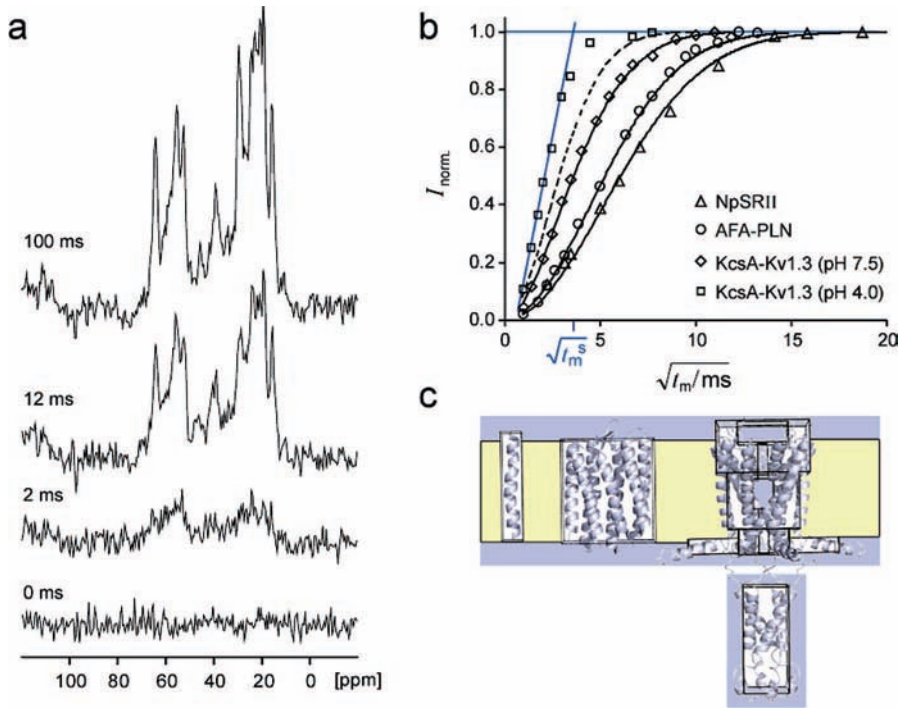

Figure 3. (a) ^{13}C detected 1D water-edited cross-polarization experiments performed for KcsA-Kv1.3 at pH 7.5 with different longitudinal proton−proton mixing times (t_m = 0, 2, 12, and 100 ms). (b) Normalized intensities obtained for 1D water-edited cross-polarization experiments plotted against the square root of mixing time t_m. The error of the data points given by the signal/noise of the integrated spectra is in the order of 2−4% for all build-up curves. Black lines represent simulated build-up curves based on 3D lattice calculations. The value $\sqrt{t_m^s}$ is obtained by a linear fit to the initial rate of the build-ups as illustrated by blue lines (see text for details). (c) Low-resolution models of AFA-PLN (left), NpSRII (middle), and KcsA-Kv1.3 (right) (black lines) are aligned to the underlying structures (gray cartoons). Lipid membrane (yellow) and water (blue) are illustrated as defined for the 3D lattice calculations.

Replacing $D \rightarrow D_{eff}$ and the indices A → W, B → P, and $I_B(t_m) \rightarrow M_P(t_m)$ in eq 3, we obtain

$$\frac{M_P(t_m)}{M_P(t_m \rightarrow \infty)} \approx \sqrt{\frac{D_{eff}}{\pi}} \frac{S_{WP}}{V_P} \sqrt{t_m} \tag{4}$$

and for the limit $M_P(t_m^s) = M_P(t_m \rightarrow \infty)$

$$\sqrt{t_m^s} = \sqrt{\frac{\pi}{D_{eff}}} \frac{V_P}{S_{WP}} \tag{5}$$

Hence, the time constant of the magnetization transfer is proportional to the molecular dimensions of the protein in close analogy to domain-size measurements performed previously for heterogeneous polymers.[19,20]

Three-Dimensional Lattice Calculations. We utilized the concept of 'diffusion on a lattice' as described by Schmidt-Rohr and Spiess (ref 18, Chapter 13.3.3) to numerically simulate the build up for protein magnetization according to eq 1. Correspondingly, a 3D lattice was constructed to reflect a low-resolution model of the protein of interest (see also Results and Discussion, Figure 3c). The corresponding spin network consists of cubes with an edge length, d, of 2 Å. Only protein segments that contribute to the cross-polarization signal were considered for the low-resolution models. Each cube was defined to be part of the protein, the lipid membrane, or the surrounding water. Magnetization transfer within the three-dimensional spin network was calculated in MATLAB using time steps, Δt_m, of 20 μs according to

$$M_{x,y,z}(t_m + \Delta t_m) = M_{x,y,z}(t_m) + \sum_i \frac{D_{ij} \Delta t_m}{d^2} (M_i(t_m) - M_{x,y,z}(t_m)) \tag{6}$$

Here, $M_i(t_m)$ monitors the magnetization of the six neighboring cubes ($x + 1$, y, z; $x - 1$, y, z; x, $y + 1$, z; x, $y - 1$, z; x, y, $z + 1$; x, y, $z - 1$), and the D_{ij} stand for the corresponding diffusion coefficients. Magnetization of water was kept constant at 1 assuming a large water pool and water bulk diffusion in the range of 10^6 nm^2/ms that is orders of magnitude faster than the observed exchange processes. In addition to magnetization transfer from water spins directly to protein spins and among protein nuclei, indirect pathways of magnetization transfer via lipid molecules may influence the measured build-up rates. To characterize the influence of the surrounding lipid bilayer, we performed water-edited experiments observing the magnetization transfer from water to the lipid tail protons of asolectin liposomes (Figure 2d). The experimental build-up curve for CH_2 lipid side chain magnetization was compared to lattice calculations considering two diffusion coefficients for water to lipid and lipid to lipid magnetization transfer. From the data, we approximate a water to lipid diffusion coefficient of about 0.001 nm^2/ms which is almost 1 order of magnitude smaller than the water to protein diffusion coefficient obtained under identical experimental conditions (see Results and Discussion). In addition, a lipid to lipid diffusion coefficient of 0.016 nm^2/ms was found. Our results are in line with earlier work reporting a lipid to lipid diffusion coefficient of 0.012 nm^2/ms, a lipid to protein diffusion coefficient of 0.0025 nm^2/ms, and a protein-to-protein diffusion coefficient of 0.3 nm^2/ms.[11] Furthermore, we find for lipid chain protons T_1 values of typically 200−500 ms while water T_1 values are between 500 and 1200 ms for all samples used in this study (see also Table 1). Therefore, magnetization transferred via lipid protons is further reduced by accelerated relaxation. In summary, we conclude that indirect pathways of magnetization transfer from water to protein via lipid spins can be neglected to first approximation. Consequently, the protein magnetization was initially set to zero, while the lipid magnetization remained zero

(19) Assink, R. A. *Macromolecules* **1978**, *11*, 1233–1237.
(20) Egger, N.; Schmidt-Rohr, K.; Blümich, B.; Domke, W. D.; Stapp, B. *J. Appl. Polym. Sci.* **1992**, *44*, 289–295.

Table 1. Diffusion and Relaxation Parameters[a]

sample	D_{PP}	D_{WP}	D_{LL}	D_{WL}	$T_1(H_2O)$	T_1(lipid)
asolectin liposomes	–	–	0.016	0.001	500	450
NpSRII	0.3	0.008	–[b]	–[b]	1200	590
AFA-PLN	0.3	0.008	–[b]	–[b]	690	350
KcsA-Kv1.3 (pH 7.5)	0.3	0.008	–[b]	–[b]	1150	250

[a] Diffusion coefficients as obtained by lattice calculations for magnetization transfer from protein to protein (D_{PP}), water to protein (D_{WP}), lipid to lipid (D_{LL}), and water to lipid (D_{WL}) (in nm^2/ms) that agree best with the experimental data and experimentally determined T_1 values for water and the CH_2 lipid tail resonance (in ms). [b] Secondary pathways for magnetization transfer from water to protein via the lipid protons were ignored in the performed 3D lattice calculations.

during the course of the lattice calculations. For all simulations, the relative protein magnetization was read out every 1 ms.

Results and Discussion

Analysis of One-Dimensional Water−Protein Transfer Curves. To study the details of the polarization transfer from water to a membrane-embedded protein, solid-state NMR experiments were recorded for proteoliposomes containing proteins of different size and different lipid compositions. In particular, sensory rhodopsin II from *Natronomonas pharaonis* (NpSRII), a monomeric phospholamban mutant (AFA-PLN) and the chimeric ion channel KcsA-Kv1.3 at pH 7.5 were investigated in a membrane setting. Bilayer preparations varied from synthetic (AFA-PLN) to purple membrane (NpSRII) lipids (Table 2).

Figure 3a shows exemplarily ^{13}C detected 1D water-edited cross-polarization experiments performed for KcsA-Kv1.3 at pH 7.5 with different longitudinal proton−proton mixing times. No signal is detected at zero mixing time confirming that residual protein magnetization can be fully suppressed by the combination of a selective initial pulse and a ^{1}H T_2 filter (τ = 1 ms). Notably, this aspect is crucial for a reliable interpretation of the build-up data. In addition, results of (selective) ^{1}H one-pulse spectra confirm the high water content of our KcsA-Kv1.3 proteoliposome preparations (Supporting Information, Figure 1). The T_1-corrected build-up curves obtained by ^{13}C detected water-edited cross-polarization experiments, in which the (^{1}H, ^{1}H) mixing time t_m was varied, are given in Figure 3b for the systems considered.

In addition, the build-up curve for KcsA-Kv1.3 at pH 4.0 is plotted in Figure 3b. Following previous work on the parent KcsA channel,[23] a change to acidic pH should lead to channel opening by rearrangement of the inner helix bundle.

In Figure 3b, solid black lines represent simulated build-up curves obtained from three-dimensional lattice calculations (see Material and Methods). In these computations, three-dimensional spin networks representing structural models of the three investigated proteins were employed. These low-resolution representations were approximated for NpSRII starting from the available crystal structure,[24] for AFA-PLN from the published solid-state NMR structure[15] and for KcsA-Kv1.3 from a structural model based on X-ray, EPR, and ssNMR data[21,25,26] (Figure 3c). To first approximation, lipid bilayers can be treated as inert diffusion barriers in the simulation due to comparatively small water to lipid and lipid to protein diffusion coefficients (D_{WL} and D_{LP}) and the small T_1 values measured for the lipids in our experiments (see Materials and Methods and Table 1). Thus, the lattice calculations depend only on two diffusion coefficients describing the efficiencies for magnetization transfer from water−protein and protein−protein spins. The source magnetization represented by water was considered to be large and the water bulk diffusion is several orders of magnitude faster than the observed transfer processes. Therefore, water magnetization was kept constant throughout the simulations. For all three systems, we found excellent agreement between experimental and simulated build-up curves investigated if a protein−protein diffusion coefficient of 0.3 nm^2/ms and a water−protein diffusion coefficient of 0.008 nm^2/ms were used. This result reflects the fact that fast intramolecular spin diffusion is redistributing the polarization from the surface rapidly within the whole protein volume. Notably, the water−protein diffusion coefficient is about 6 times smaller than the value used in previous contributions.[9,10] Considering that these measurements were performed at significantly lower temperatures in the range of 240 K compared to 280 K used in our experiments, this difference can be attributed to the temperature dependence of the molecular dynamics of protein segments involved in the magnetization transfer from water to protein. Furthermore, the relative contribution of the polarization transfer mechanisms might change significantly with temperature. On the other hand, the protein−protein diffusion coefficient is only decreased by about 25% for our simulations, suggesting that the overall protein dynamics are comparable in all studies.

By linear extrapolation of the initial rate to 100% magnetization we obtain the value t_m^s (Figure 3b) which describes the transfer characteristics away from saturation conditions.[18] The correlation coefficients for linear fits to the initial rate of magnetization transfer are 0.995, 0.996, and 0.998 for KcsA-Kv1.3, SRII, and AFA-PLN, respectively. At time t_m^s, eq 4 equals 1 and we obtain a linear dependence between the square root of t_m^s and the volume to surface ratio given in eq 5. This dependence is in good agreement with the plot of volume to surface ratios determined for the low resolution models compared to experimental values for the square root of t_m^s shown in Figure 4a. Hence, an effective diffusion coefficient for the magnetization transfer from water to membrane proteins of about 0.2 nm^2/ms can be derived that establishes a general parameter to monitor V_p/S_{WP} by ssNMR.

While the error associated with t_m^s mainly depends on the signal-to-noise ratio of the evaluated spectra, judging the error of the volume to surface ratio is difficult. The volume per amino acid is 0.10 ± 0.01 nm^2 for the three low-resolution models investigated. This suggests that the protein volume can be approximated quite accurately on the basis of protein size. However, the definition of the water-accessible surface depends on the lipid bilayer thickness and the surface itself is inaccurate due to the three-dimensional shape of the spin network.

In order to verify the accuracy of the low-resolution models used for the lattice calculations, we employed the VADAR Web Server[22] to obtain volume and water accessible surfaces for the

(21) Schneider, R.; Ader, C.; Lange, A.; Giller, K.; Hornig, S.; Pongs, O.; Becker, S.; Baldus, M. *J. Am. Chem. Soc.* **2008**, *130*, 7427–7435.
(22) Willard, L.; Ranjan, A.; Zhang, H.; Monzavi, H.; Boyko, R. F.; Sykes, B. D.; Wishart, D. S. *Nucleic Acids Res.* **2003**, *31*, 3316–3319.
(23) Liu, Y.-S.; Sompornpisut, P.; Perozo, E. *Nat. Struct. Mol. Biol.* **2001**, *8*, 883–887.
(24) Royant, A.; Nollert, P.; Edman, K.; Neutze, R.; Landau, E. M.; Pebay-Peyroula, E.; Navarro, J. *Proc. Natl. Acad. Sci.* **2001**, *98*, 10131–10136.
(25) Zhou, Y.; Morais-Cabral, J. H.; Kaufman, A.; MacKinnon, R. *Nature* **2001**, *414*, 43–48.
(26) Cortes, D. M.; Cuello, L. G.; Perozo, E. *J. Gen. Physiol.* **2001**, *117*, 165–180.

Table 2. Key Data for NpSRII, AFA-PLN, and KcsA-Kv1.3[a]

	lipids	no. res.	mobile res.	no. protons	V_P	S_{WP}	H−H dist.	no. cubes	V_P^{mod}	S_{WP}^{mod}	t_m^s
NpSRII	purple membane	249	∼44	∼1810	28.6	38.5	2.51	2880	23.0	11.5	135
AFA-PLN	DMPC	54	∼28	∼260	3.4	6.6	2.34	336	2.7	1.9	90
KcsA-Kv1.3	asolectin	640	∼0	∼5000	43.1	235.6	2.05	7397	59.2	88.2	40

[a] Lipid composition of the investigated proteoliposomes, total number of amino acid residues (no. res.), approximate number of mobile residues that do not contribute to the cross-polarization spectra (mobile res.),[12,15,21] approximate number of rigid protons (no. protons), protein volume in nm^2 according to VADAR[22] (V_P), water accessible surface of the protein in nm^2 according to VADAR (S_{WP}), average proton−proton distance in Å defined as (*V*/no. protons)$^{1/3}$ (H−H dist.), number of 2 Å cubes of the low resolution model (no. cubes), volume of the low resolution model in nm^2 (V_P^{mod}), water accessible surface of the low-resolution model in nm^2 (S_{WP}^{mod}), and initial rate saturation time in ms (t_m^s).

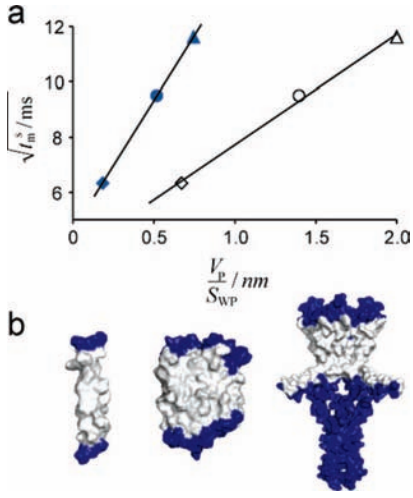

Figure 4. (a) Plot of experimentally determined values for $\sqrt{t_m^s}$ versus volume to water-accessible surface ratios calculated based on the low-resolution models of KcsA-Kv1.3 (◊), AFA-PLN (○), and NpSRII (Δ) and based on the underlying structures of KcsA-Kv1.3 (♦), AFA-PLN (●), and NpSRII (▲). Straight lines give linear fits to the data (R^2(low resolution) = 0.997 and R^2(structures) = 0.999). (b) Surface representations of AFA-PLN (left), NpSRII (middle), and KcsA-Kv1.3 (right). Residues defined to be water accessible are labeled blue.

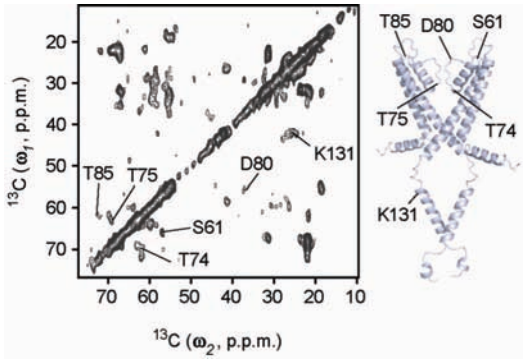

Figure 5. Water-edited initial regime (^{13}C, ^{13}C) correlation spectrum for KcsA-Kv1.3 at pH 7.5. Selected cross peaks representing extracellular turret, C-terminus, and selectivity filter are labeled and indicated in the structural model (only two subunits are shown). Note that resonance were only considered if unambiguous in terms of the chemical-shift values and if present on both sides of the diagonal.

underlying protein structures and structural models. The total volume of the protein is calculated as the sum of the space enclosed by the van der Waals surfaces of all residues. Residues contributing to the water accessible surface were selected based on existing data[12,15,21] (Figure 4b, 5) and the surface area was computed by summing up accessible surface areas identified by VADAR for residues that contribute to the defined water−protein interface. Table 2 summarizes dimensional parameters obtained for the low-resolution models and the underlying structures. The volumes of the low-resolution models deviate by 20−30% from the van der Waals volume analysis confirming that the low-resolution models provide a reasonable approximation for the proteins considered.

Changes in reference to the protein surface should only mildly affect the residual protein−protein diffusion coefficient. According to Table 2, the calculated average proton−proton distances give values close to 2 Å, which is line with our numerical analysis. Starting from the protein−protein diffusion coefficient D_{PP} of 0.3 nm^2/ms, we can estimate the transfer rate of magnetization, Ω, between two protons $a = 2$ Å apart to be 7.5 kHz according to $\Omega = D_{PP}/a\Omega$. This value is in good agreement to earlier studies studying carbon-detected proton−proton mixing under MAS conditions.[27] On the other hand, the surface areas of our low-resolution models and structures differ on average by a factor of 3.2 ± 0.4 reflecting the different levels of surface complexity. Therefore, the protein surfaces are underestimated in the simulations or, correspondingly, the water to protein diffusion coefficient is overestimated in the lattice calculations. Plotting the square root of t_m^s against the volume to surface ratio obtained based on the van der Waals radii yields a linear dependency suggesting an effective diffusion coefficient for water−protein magnetization transfer of 0.04 nm^2/ms (Figure 4a). This value is five times smaller than the effective diffusion coefficient obtained based on the low-resolution models in line with the discrepancy in water accessible surface areas. By simulating the magnetization transfer in spin networks of various volume-to-surface ratios, we can show that the larger water accessible surface of the van der Waals representations correlates linearly with a decrease in the water−protein diffusion coefficient (Supporting Information, Figure 2). Thus, the actual water−protein polarization transfer rate at the given temperature of 280 K should be on average 60 Hz, providing an overall estimate of the transfer rate for magnetization transfer from water to protein. Such a value is both compatible with ^{1}H−^{1}H dipolar couplings and chemical exchange processes. Local transfer rates involving individual spin pairs may, however, differ significantly. In this context it might be important to point out that the fraction of amino acid residues having exchangeable protons in addition to the backbone amides ranges from 25% to 55% in the water-accessible surfaces as defined in Figure 4b.

Two-Dimensional, Residue-Specific Analysis. In line with our recent work on NpSRII,[12] our analysis of 1D transfer dynamics confirms that 2D water-edited (^{13}C, ^{13}C) correlation experiments measured in the initial regime (2.5 ms (^{1}H, ^{1}H) mixing time) can provide residue-specific information about the H_2O-accessible protein surface. In the case of KcsA-Kv1.3 at pH 7.5 (Figure 5), we find that the water-accessible protein surface comprises residues in the extracellular turret and the C-terminal

(27) Lange, A.; Seidel, K.; Verdier, L.; Luca, S.; Baldus, M. *J. Am. Chem. Soc.* **2003**, *125*, 12640–12648.

helices of the potassium channel. In addition, we can unambiguously assign resonances that originate from the lower part of the selectivity filter including Thr74 and Thr75. The Cα−Cβ cross-peak intensities of these residues are comparable to values seen for Thr85 which is located in the turret of KcsA-Kv1.3. Residue-specific 3D lattice calculations (Supporting Information, Figure 3) show that this finding is compatible with a water-accessible selectivity filter and rule out a selectivity filter conformation that is remote from fast exchanging water. It should be mentioned that such an analysis is not possible for larger mixing times t_m as spin-diffusion rapidly distributes magnetization throughout the protein. Under such conditions, the use of deuterated protein samples and transversal mixing periods may be helpful.[28] Comparing experiment and simulation, we conclude that selectivity filter and inner cavity of the channel are accessible to water on the time scale relevant for our experiment. This is especially notable as solvent accessibility of the selectivity filter and the inner cavity has mostly been discussed on the basis of molecular dynamics simulations.[29,30]

Channel Opening As Seen by Water-Edited ssNMR. Sizeable structural changes, for example as expected in response to KcsA-Kv1.3 channel opening by changes in pH, should influence H_2O-edited ssNMR experiments. Indeed, using eq 5, the experimentally determined values for $\sqrt{t_m^s}$, and constant protein volumes we can readily compute an increase in water-accessible surface area of KcsA-Kv1.3 by about 65% if pH is brought from pH 7.5 to 4.0. The interpretation of relative changes in water-accessible surface has the advantage that the effective diffusion coefficient D_{eff} can be eliminated, and thus, the results obtained do not depend on the errors introduced by the definition of the low-resolution models and the water-accessible surface areas. Figure 6a shows the pH-dependent change of the square root of the initial rate 100% time t_m^s for KcsA-Kv1.3.

The data can be fitted to the Hill equation if we consider the obtained saturation times to be an average for two states of the channel, i.e., one closed and one opened state. We obtain a Hill coefficient of 1.0 ± 0.2 and a pK_a value of 6.0 ± 0.3. These values compare favorably to results obtained on the parent KcsA K^+ channel by measuring the pH dependence of $^{86}Rb^+$ influx under similar conditions.[26] On the basis of crystal structures of open potassium channels such as MthK[31] and Kv1.2,[32] as well as a recent ssNMR study of KcsA-Kv1.3,[33] we approximated a low-resolution model for the open pore domain—omitting N- and C-terminus—for KcsA-Kv1.3 at pH 4.0 (Figure 6b). Compared to the low-resolution model for the closed potassium channel at pH 7.5 the water accessible protein surface is increased by about 50%. The simulated build-up curve for this model is given as dashed line in Figure 2b. It is obvious that this model does not fully account for the increase in water accessible protein surface observed experimentally. However, the degree of change agrees well with the notion that channel opening is associated with a structural rearrangement leading to a major increase in pore diameter and possibly also affects the water accessibility of C- and N-terminus of the potassium channel.

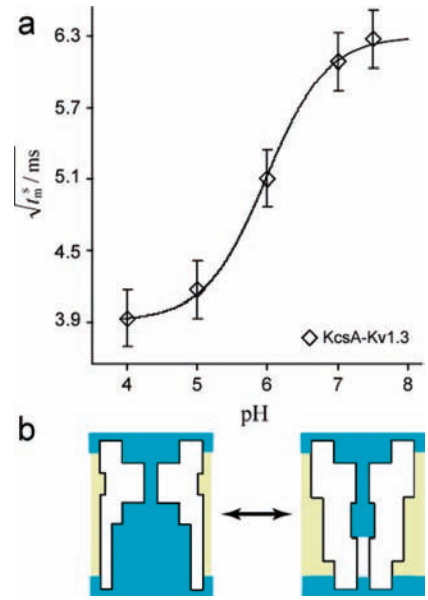

Figure 6. (a) Plot of the square root of experimentally determined initial rate 100% values t_m^s for KcsA-Kv1.3 against pH. Error bars represent signal/noise of the evaluated 1D spectra. (b) Cross-section of the low-resolution models for the opened and closed pore domain of KcsA-Kv1.3. Lipid membrane (yellow) and water (blue) are illustrated as defined for the 3D lattice calculations.

Conclusions

Water-edited solid-state NMR experiments allow for probing the water−protein surface in reference to the protein volume of large membrane proteins in close analogy to domain-size measurements performed previously for heterogeneous polymers.[19,20] Here, we have reported effective diffusion coefficients that allow for computation of H_2O surface-to-volume ratios based on the time constant t_m^s describing magnetization transfer from water to protein. Such an analysis is possible for both low-resolution models suitable for lattice calculations and protein structures if high-resolution information is available. Low-resolution models may permit to distinguish different membrane protein topologies and help to estimate the magnitude of structural rearrangements as demonstrated for KcsA-Kv1.3. In general, the error associated with the low-resolution model should decrease with protein size making the analysis more favorable for large proteins or protein complexes. If high-resolution structural information is available, water-edited ssNMR spectroscopy might serve as a qualitative means to elucidate 3D molecular structure in membranes under variable experimental conditions such as lipid type or composition.

Isotope-labeling of the protein in combination with 2D spectroscopy offers a sensitive means to examine the H_2O-accessible surface of the protein on the atomic level. Notably, such information can also be obtained in other macromolecular systems[34] and the data can be analyzed in a manner comple-

(28) Böckmann, A.; Juy, M.; Bettler, E.; Emsley, L.; Galinier, A.; Penin, F.; Lesage, A. *J. Biomol. NMR* **2005**, *32*, 195–207.
(29) Bernèche, S.; Roux, B. *Biophys. J.* **2000**, *78*, 2900–2917.
(30) Boiteux, C.; Kraszewski, S.; Ramseyer, C.; Girardet, C. *J. Mol. Model.* **2007**, *13*, 699–713.
(31) Jiang, Y.; Lee, A.; Chen, J.; Cadene, M.; Chait, B. T.; MacKinnon, R. *Nature* **2002**, *417*, 523–526.
(32) Long, S. B.; Campbell, E. B.; MacKinnon, R. *Science* **2005**, *309*, 897–903.
(33) Ader, C.; Schneider, R.; Hornig, S.; Velisetty, P.; Wilson, E. M.; Lange, A.; Giller, K.; Ohmert, I.; Martin-Eauclaire, M.-F.; Trauner, D.; Becker, S.; Pongs, O.; Baldus, M. *Nat. Struct. Mol. Biol.* **2008**, *15*, 605–612.
(34) Andronesi, O. C.; Bergen, M. v.; Biernat, J.; Seidel, K.; Griesinger, C.; Mandelkow, E.; Baldus, M. *J. Am. Chem. Soc.* **2008**, *130*, 5922–5928.

mentary to EPR studies using solvent accessibility data.[35,36] In addition, structural changes in response to function can be followed on the global and local scale. In the case of pH-induced opening of the KcsA-Kv1.3 channel, the calculated increase in water-accessible surface area of the K^+ channel is in line with crystal structures of other opened potassium channels. Furthermore, the pH dependence of channel opening could be followed on a direct structural basis in a titration experiment. The resulting Hill coefficient is in good agreement with biochemical data for the parent potassium channel KcsA underlining the potential of ssNMR to directly relate protein structure to function in a membrane setting.

(35) Hubbell, W. L.; Cafiso, D. S.; Altenbach, C. *Nat. Struct. Mol. Biol.* **2000**, *7*, 735–739.
(36) Sompornpisut, P.; Roux, B.; Perozo, E. *Biophys. J.* **2008**, *95*, 5349–5361.

Acknowledgment. Technical assistance by K. Giller, S. Martell, and B. Angerstein is gratefully acknowledged. We thank Professors M. Engelhard and O. Pongs for stimulating discussions. This work was funded in part by the DFG (Ba 1700/5-1), by a Kekule fellowship to C.A. from the Stiftung Stipendien-Fonds of the Verband der Chemischen Industrie, and by a Ph.D. fellowship to R.S. from the DFG graduate school 782 "Spectroscopy and Dynamics of Molecular Coils and Aggregates".

Supporting Information Available: ^{1}H spectra, comparison of values for $\sqrt{t_m}^s$ obtained by simulation of various spin networks with the linear dependencies given in Figure 4a, and residue specific lattice calculations for Thr75 and Thr85. This material is available free of charge via the Internet at http://pubs.acs.org.

JA806306E